Nano Research
2023, 16(5): 7337–7346

ISSN 1998-0124 CN 11-5974/O4
https://doi.org/10.1007/s12274-023-5395-6

Research Article

Self-assembled multiepitope nanovaccine based on NoV P particles induces effective and lasting protection against H3N2 influenza virus

Jiaojiao Nie[1], Qingyu Wang[1], Shenghui Jin[1], Xin Yao[1], Lipeng Xu[1], Yaotian Chang[1], Fan Ding[1], Zeyu Li[1], Lulu Sun[1], Yuhua Shi[1], and Yaming Shan[1,2] (✉)

[1] *National Engineering Laboratory for AIDS Vaccine, School of Life Sciences, Jilin University, Jilin 130012, China*
[2] *Key Laboratory for Molecular Enzymology and Engineering, The Ministry of Education, School of Life Sciences, Jilin University, Jilin 130012, China*

Received: 26 October 2022 / **Revised:** 4 December 2022 / **Accepted:** 8 December 2022

ABSTRACT

Current seasonal influenza vaccines confer only limited coverage of virus strains due to the frequent genetic and antigenic variability of influenza virus (IV). Epitope vaccines that accurately target conserved domains provide a promising approach to increase the breadth of protection; however, poor immunogenicity greatly hinders their application. The protruding (P) domain of the norovirus (NoV), which can self-assemble into a 24-mer particle called the NoV P particle, offers an ideal antigen presentation platform. In this study, a multiepitope nanovaccine displaying influenza epitopes (HMN-PP) was constructed based on the NoV P particle nanoplatform. Large amounts of HMN-PP were easily expressed in *Escherichia coli* in soluble form. Animal experiments showed that the adjuvanted HMN-PP nanovaccine induced epitope-specific antibodies and haemagglutinin (HA)-specific neutralizing antibodies, and the antibodies could persist for at least three months after the last immunization. Furthermore, HMN-PP induced matrix protein 2 extracellular domain (M2e)-specific antibody-dependent cell-mediated cytotoxicity, $CD4^+$ and $CD8^+$ T-cell responses, and a nucleoprotein (NP)-specific cytotoxic T lymphocyte (CTL) response. These results indicated that the combination of a multiepitope vaccine and self-assembled NoV P particles may be an ideal and effective vaccine strategy for highly variable viruses such as IV and SARS-CoV-2.

KEYWORDS

self-assemble, norovirus protruding (NoV P) particle, influenza virus, multiepitope, nanovaccine

1 Introduction

In a world still fighting the SARS-CoV-2 pandemic, the threat from seasonal and pandemic influenza persists [1, 2]. According to the estimate of World Health Organization (WHO), annual influenza epidemics cause 3 to 5 million illnesses and 290,000 to 650,000 deaths and impose a huge public health and economic burden worldwide [3, 4]. Currently, annual seasonal influenza vaccination remains the most effective measure to prevent and control influenza epidemics, although its production is complex and time-consuming [5]. Most seasonal influenza vaccine strains are cultured in chicken embryos, which may lead to adaptive mutations in the virus and consequent safety issues [6–8]. In addition, due to the antigenic drift and antigenic shift of influenza virus (IV), seasonal vaccines have to be reformulated annually according to WHO-recommended formulations of strains [9]. However, seasonal vaccines have the inevitable risk of mismatch between the vaccine and the circulating strains, resulting in a relatively narrow scope of protection [10]. Therefore, there is an urgent worldwide need to develop a safe and effective "universal" influenza vaccine (UIV) against most influenza viruses.

Studies have established that the sequences of the haemagglutinin stalk domain (HA2), matrix protein (M1), matrix protein 2 extracellular domain (M2e), and nucleoprotein (NP) of IV are highly conserved among strains, making them potential targets for UIVs [11, 12]. Many vaccine platforms have also been used to develop UIVs to address the inadequacies of seasonal influenza vaccines [13], such as virus-like particles (VLPs) [14–17], epitope vaccines [18–20], nucleic acid-based vaccines [21–23], and viral vector vaccines [24–28]. For other next-generation influenza vaccines, epitope vaccines have an opportunity to focus immune responses on conserved epitopes to improve efficacy and breadth of protection [29]. Moreover, it has the potential to induce strong immune responses to nondominant or cryptic epitopes in natural immune processes by precisely targeting antigens [30]. The manufacturing process is simple, low cost, and suitable for large-scale production. Influenza epitope vaccines might be a promising strategy for the development of safe and effective UIVs.

Despite its undeniable advantages, the development of a conserved domain as a UIV candidate is still hampered by its low immunogenicity [31]. It is necessary to develop a potent epitope-displaying carrier to enhance its immunogenicity [30]. Recently, self-assembled nanocarriers have attracted great attention in the development of vaccines because of their good biocompatibility and surface modifiability [32–35]. Many vaccine candidates based on self-assembled nanocarriers have elicited markedly broader and more potent immune responses than either soluble antigens unconjugated to nanocarriers or traditional vaccines, including

Address correspondence to shanym@jlu.edu.cn

phosphorylated Tau [36], M2e [37], and enterovirus 71 (EV71) epitopes [38]. The protruding (P) domain of capsid protein VP1 of norovirus (NoV) can be stably expressed in *Escherichia coli* as soluble proteins on a large scale and self-assemble into three convertible forms. Among the three forms, the 24-mer P particles (NoV P particles) are the most suitable as vaccine carriers to enhance the immunogenicity and stability of antigens [39]. The three surface loops on the P domain can be modified to display foreign antigens [40, 41]. In our previous research, NoV P particles with multiple HA2 epitopes on the exterior surface induced strong and specific immune responses against each epitope [20]. In brief, the NoV P particle is an ideal nanocarrier for epitope display because of its high stability, nontoxicity, low cost, and surface modifiability.

In this study, we fused the conserved linear epitopes of HA2, M2e, and NP to three surface loops on the P domain and designed a multiepitope nanovaccine termed HMN-PP. After prokaryotic expression and affinity purification, we characterized the multiepitope nanovaccine *in vitro* and evaluated its ability to elicit potent and long-term immune responses against IV *in vivo*. The multiepitope nanovaccines based on NoV P particle in this study might represent a promising technology for the development of UIVs.

2 Experimental

2.1 Cells, peptides, genes, viruses, and animals

Raji cells and Madin Darby canine kidney (MDCK) cells were obtained from the American Type Culture Collection (ATCC; MD, USA). Briefly, Raji cells were grown in RPMI 1640 medium (Gibco) containing 10% fetal bovine serum (FBS; Gibco) and sodium pyruvate. MDCK cells were maintained under adherent culture conditions in Dulbecco's modified Eagle's medium (DMEM; Gibco) with 10% FBS. All cell lines were maintained in a T-flask at 37 °C in a humidified atmosphere of 5% CO_2. All peptides, such as H16 (DLWSYNAELLVALENQ), M2e (SLLTEVETPIRNEWGCRCNDSSD), and NP9 (LPFERATVM), were chemically synthesized by GL Biochem (Shanghai) Ltd. (95% purity). All genes used in this study were codon-optimized and gene-synthesized by Nanjing GenScript Biological Technology & Service (China). All influenza strains (A/17/Perth/16/2009(H3N2), A/Hong Kong/2671/2019(H3N2), A/Guangdong-Maonan/SWL1536/2019(H1N1), A/17/California/2009/38 (H1N1), and B/60/Massachusetts/20/2012) were kindly provided by Changchun BCHT Pharmaceutical Co., Ltd. (Jilin, China). BABL/c mice (female, six- to eight-week-old, weighing 18–20 g, and specific pathogen free (SPF)) were procured from Liaoning Changsheng Biotechnology Co., Ltd. (Liaoning, China). All procedures were in accordance with the Regulations for the Administration of Affairs Concerning Experimental Animals approved by the State Council of People's Republic of China, and all animal protocols were approved by the Institutional Animal Care and Use Committee of Jilin University (approval numbers 2021YNSY0903 and 2021YNSY0703).

2.2 Design and preparation of nanoparticles

The gene of the NoV (GenBank: DQ078814.2) P domain was cloned into the pET20b (+) vector between the *Nde I* and *Xho I* sites with a C-terminal His-tag, resulting in pET-20b-PP. The epitope gene was inserted into the loops of the NoV P domain through the restriction sites *Kpn I* and *Eag I*. The single-copy H16, M2e, and NP9 epitopes were inserted into the three loops of the NoV P domain to construct a recombinant plasmid, named HMN-PP. To construct the control plasmids, three identical epitopes, H16, M2e, and NP9, were simultaneously inserted into three loops of the NoV P domain, resulting in H16-PP, M2e-PP, and NP9-PP, respectively.

Five successfully constructed recombinant plasmids were transformed into *E. coli* BL21 (DE3) pLysS competent cells. When the *E. coli* culture entered the logarithmic phase of growth, 0.1 mM isopropylthio-β-d-galactoside (IPTG) was added to induce protein expression for another 12 h at 16 °C. The harvested cells were re-suspended in TBS buffer (50 mM Tris, 150 mM NaCl, pH 8.0) and disrupted by sonication at 4 °C. The recombinant NoV P particles were purified from the culture supernatant by affinity chromatography on a His-trap column (GE Healthcare, USA).

2.3 Characterization of nanoparticles based on NoV P particle

The purified nanoparticles based on NoV P particle were analysed by SDS-PAGE with Coomassie brilliant blue staining. The size distribution of nanoparticles was evaluated by dynamic light scattering (DLS) on a Zetasizer Nano ZS90 (Malvern Instruments, UK). The typical structure of nanoparticles was investigated by transmission electron microscopy (TEM; H-7650, Hitachi, Japan) at an acceleration voltage of 100 kV.

2.4 Animal immunization

Female BALB/c mice were randomly divided into 6 groups (n = 24/group) and immunized as follows: PBS (negative control), PP (negative control), H16-PP, M2e-PP, NP9-PP, and HMN-PP. 30 μg of purified nanoparticle was mixed at a volume ratio of 3:1 with Imject alum adjuvant (Thermo Fisher Scientific) for a total volume of 200 μL. Mice were immunized subcutaneously (s.c.) three times at two-week intervals. Sera samples were collected at week 0, 2, 4, 6, 10, and 16 after immunization, separated, and stored at −20 °C until further analysis.

2.5 Enzyme linked immunosorbent assay (ELISA)

For specific antibody detection of peptides, 96-well plates were coated with H16 peptide, M2e peptide, or NP9 peptide (3 μg/mL) in coating buffer, incubated overnight at 4 °C, and washed with PBST (0.05% Tween-20 in PBS). Subsequently, the plates were blocked with 5% bovine serum albumin (BSA) in PBS for 2 h at 37 °C. Following three washes, serially diluted sera was added to the wells and incubated for 1.5 h at 37 °C. After five washes with PBST, horseradish peroxidase (HRP)-conjugated goat anti-mouse IgG antibody was added and incubated for another 45 min. Plates were washed with PBST, and subsequently developed with TMB (Tiangen Biotech, Beijing, China) for 20 min in the dark. Reaction was stopped by adding 2M H_2SO_4 and the absorbance was measured at 450 nm on an iMarK™ Microplate Reader (Bio-Rad, USA).

Antibody isotyping assay was measured to assess any changes in the Th1/Th2 balance. Coating, blocking, and primary antibody incubation were performed as described above. Goat anti-mouse IgG1 and IgG2a subclass antibodies (Sigma) were added as the secondary antibodies and incubated for 45 min at room temperature. Alkaline phosphatase (AP)-conjugated anti-goat IgG antibody (Beijing Dingguo Inc.) was added as the tertiary antibody and incubated for 30 min at room temperature. After color development in p-nitrophenyl phosphate substrate (PNPP; Sigma), reaction was stopped with 3 M NaOH and the absorbance was measured at 405 nm.

2.6 Microneutralization (MN) assay

The day before the MN assay, MDCK cells (1×10^5/well) were

seeded into 96-well culture plate. Serial dilutions of sera were mixed with 100-fold $TCID_{50}$ of virus for 2 h at 37 °C. The virus-serum mixture was then added to the 96-well culture plate coated with MDCK and incubated for 48 h to observe the cytopathic effect (CPE). Microneutralization titers (ID_{50}) were expressed as the reciprocal serum dilution that caused 50% inhibition of virus infection.

2.7 Antibody-dependent cellular cytotoxicity (ADCC)

The day before the ADCC assay, Raji cells were incubated with 100-fold $TCID_{50}$ of A/Hong Kong/2671/2019(H3N2) virus for 12 h. Then, Raji cells were harvested and labelled with carboxyfluorescein diacetate succinimidyl ester (CFSE; Invitrogen) as target cells. Raji target cells (1×10^5 cells) were incubated with the serum (diluted 1:1000) for 1 h at 37 °C. The cells in the culture medium were used as a negative control, that is, spontaneous lysis. The cells treated with 1% Triton X-100 were used as a positive control. The cell-serum mixture was then added to the isolated effector cells at a quantity ratio of 1:10 and incubated at 37 °C for 3 h. All cells were stained with propidium iodide (PI; BioLegend) and analysed by flow cytometry (CytoFLEX cytometer, Beckman Coulter, USA). Percent ADCC activity was calculated as follows: Percent ADCC activity = [(percent experimental lysis − percent spontaneous lysis)/(percent positive control lysis − percent spontaneous lysis)] × 100%.

2.8 Lymphocyte proliferation assay

Splenocytes isolated from immunized mice were added at 2×10^5 cells/well to 96-well culture plate. Then cells were stimulated with relevant peptides (10 μg/mL) for 72 h at 37 °C. Cell proliferation was measured by MTT assay. Briefly, after treatment, 20 μL of MTT (5 mg/mL) was added to the wells and incubated for another 4 h in the dark, 100 μL of dimethyl sulfoxide (DMSO) was added after removing the supernatant carefully, and the absorbance was measured at 490 nm. The stimulation index (SI) was defined as the ratio of the optical density at 490 nm of stimulated wells to that of unstimulated wells.

2.9 T cell activation assay

Briefly, splenocytes isolated from immunized mice were blocked with anti-mouse CD16/32 antibody (BioLegend, USA), followed by staining with FITC anti-mouse CD3, PE anti-mouse CD4, and APC anti-mouse CD8α antibodies (BioLegend, USA). After washing and resuspending in cell staining buffer, cellular fluorescence was measured by flow cytometry.

2.10 Enzyme-linked immunosorbent spot (ELISpot) assay

The interferon-gamma (IFN-γ) and interleukin-4 (IL-4) ELISpot kits (Dakewe, China) were used according to the manufacturer's instructions. Briefly, splenocytes isolated from immunized mice were added at 1×10^5 cells/well to ELISpot plates that were pre-coated with the anti-mouse IFN-γ or IL-4 antibody. Cells were stimulated with peptides (10 μg/mL) for 24 h at 37 °C. Biotin-conjugated anti-IL-4 or anti-IFN-γ detection antibody, streptavidin-HRP, and AEC substrate solution were added to ELISpot plates sequentially. Spots were counted using the cytotoxic T lymphocyte (CTL) ImmunoSpot Analyzer (Cellular Technology Ltd, Cleveland, OH, USA) with ImmunoSpot software.

2.11 *In vivo* CTL assay

Lymphocytes from naïve mice were divided into two equal parts. One part was incubated with relevant peptides (10 μg/mL) for 2 h and then labelled with 5 μM CFSE as target cells. The other part was not treated with peptides and only labelled with a lower concentration (0.5 μM) of CFSE as control cells. Equal numbers of cells (1×10^7 cells) from the two parts were mixed and transferred via the tail vein into immunized mice. Twelve hours later, the mice were sacrificed, and the splenocytes were isolated and analysed by flow cytometry. Specific lysis was calculated as follows: Percentage of specific lysis = $[1 - (\text{ratio}_{control}/\text{ratio}_{experimental})] \times 100\%$, where ratio = $\%CFSE_{low}/\%CFSE_{high}$.

2.12 Virus challenge

Two weeks after the last immunization, six mice in each group were anaesthetized with sodium pentobarbital and intranasally challenged with 50 μL of a suspension containing 1×10^7 EID_{50} of A/Hong Kong/2671/2019(H3N2). Mice were monitored daily for 14 days for body weight change and survival and euthanized when they lost more than 25% of their initial body weight according to the IACUC protocol. One mouse randomly selected from each group was sacrificed 4 days post-challenge, and lung tissue was harvested and stained with haematoxylin and eosin (H&E) for histopathological evaluation.

2.13 Statistical analysis

All data were presented as the mean ± standard deviation (SD) unless otherwise indicated and were evaluated using GraphPad Prism 8.0 (GraphPad Software). Ordinary one-way analysis of variance (ANOVA) was used to compare differences between groups. Statistical significance was determined by Tukey's multiple comparisons test unless otherwise stated (indicated as follows: *, $0.01 < p < 0.05$; **, $p < 0.01$; ***, $p < 0.001$; and ns, not statistically significant).

3 Results and discussion

3.1 Epitope analysis and plasmid design

In previous studies, we screened and verified the H3N2-HA2 (residues 90–105) epitope H16 which can induce neutralizing antibodies [19]. The H16 epitope was highly conserved in the H3N2 subtype, and the conservation of each amino acid site was more than 99% (Fig. 1(a)). According to a previous method, the conserved epitope of NP (residues 418–426) of H1N1 was screened and named NP9 (Fig. 1(b)). Similarly, the conserved epitope of M2e (residues 2–24) of H3N2 was screened and named M2e. M2e was highly conserved among the H3N2 subtypes, except for positions 10, 15, and 22, where amino acid conservation was less than 95% (Fig. 1(c)). The above three epitopes were inserted into three loops of the P domain individually or in combination to construct recombinant plasmids (Figs. 1(d) and 1(e)).

3.2 Characterization of self-assembled NoV P particles *in vitro*

Soluble recombinant NoV P particles were expressed in *E. coli* and purified by nickel affinity chromatography. Protein molecular weight and purity were identified by SDS-PAGE and Coomassie blue staining (Fig. 2(a)). The molecular weights of PP, H16-PP, M2e-PP, NP9-PP, and HMN-PP were approximately 35, 45, 46, 41, and 44 kD, respectively, which were consistent with the theoretical values. All recombinant proteins were more than 95% pure and were used for further animal experiments. To further determine whether the recombinant proteins could self-assemble into nanoparticles, the size, morphology, and structure of the recombinant proteins were determined by DLS and TEM. The

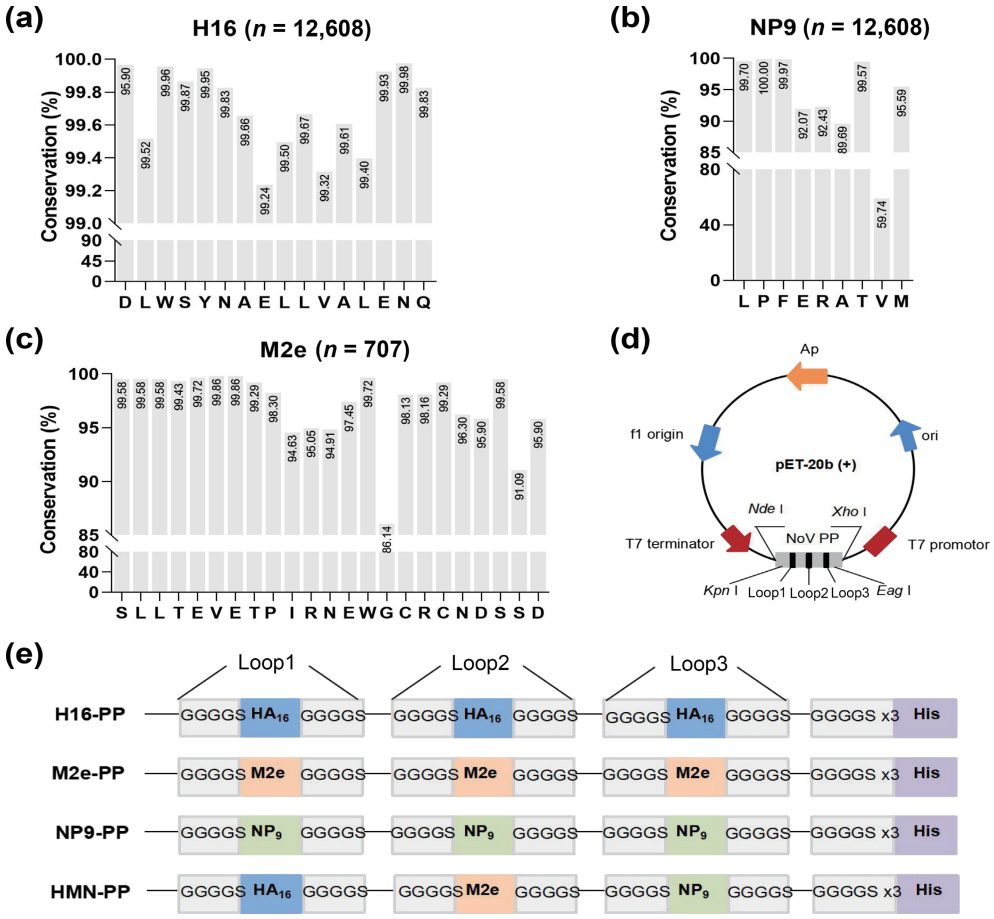

Figure 1 Sequence conservation analysis and epitope vaccine design. (a) H16 (HA2: 90–105) sequence from H3N2 (n = 12,608). (b) NP9 (NP: 418–426) sequence from H1N1 (n = 3723). (c) M2e (M2e: 2–24) sequence from H3N2 (n = 707). The plot shows the sequence conservation level in bits (sequence logo) and percentages (histogram). (d) and (e) Schematics of constructed multiepitope nanoparticles, including H16-PP, M2e-PP, NP9-PP, and HMN-PP.

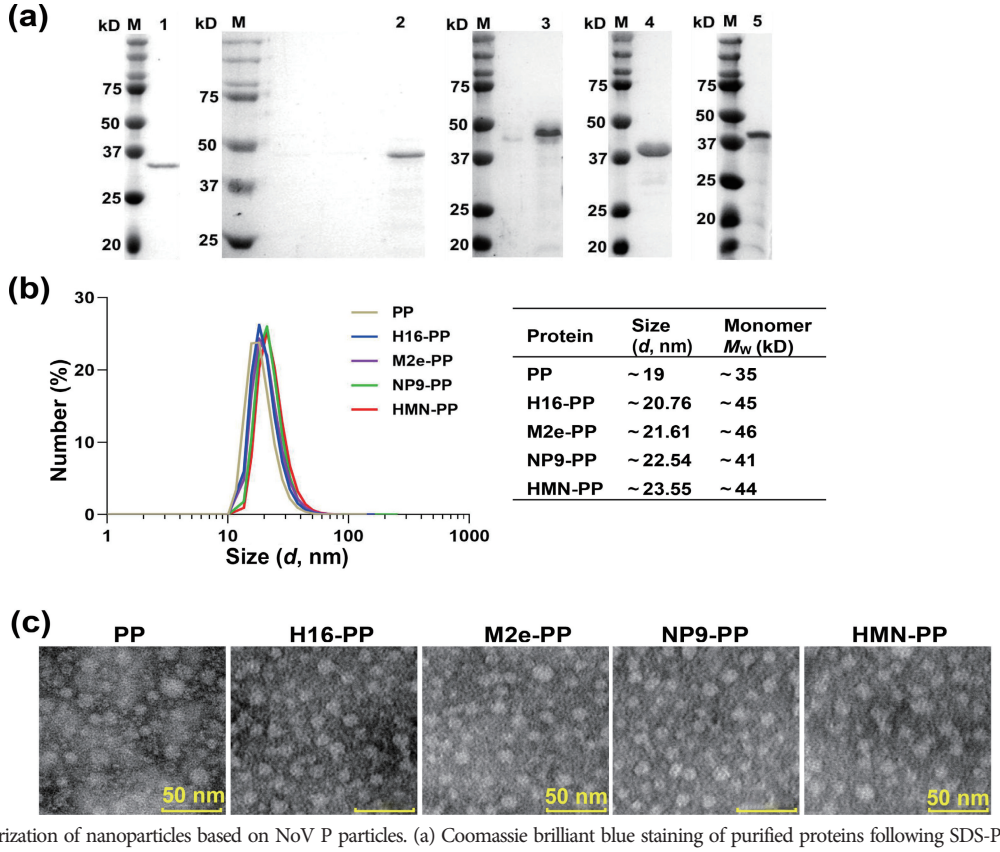

Protein	Size (d, nm)	Monomer M_W (kD)
PP	~19	~35
H16-PP	~20.76	~45
M2e-PP	~21.61	~46
NP9-PP	~22.54	~41
HMN-PP	~23.55	~44

Figure 2 Characterization of nanoparticles based on NoV P particles. (a) Coomassie brilliant blue staining of purified proteins following SDS-PAGE. M: molecular weight markers with sizes indicated in kD, lane1: PP; lane 2: H16-PP; lane 3: M2e-PP; lane 4: NP9-PP; and lane 5: HMN-PP. (b) Size distribution analysis of purified proteins by DLS (left). Particle size and protein monomer molecular weight are presented in the table (right). (c) TEM images of nanoparticles.

sizes of PP, H16-PP, M2e-PP, NP9-PP, and HMN-PP were approximately 19, 20.76, 21.62, 22.54, and 23.61 nm, respectively (Fig. 2(b)). TEM images showed that PP, H16-PP, M2e-PP, NP9-PP, and HMN-PP self-assembled into near-spherical protein nanocages with a diameter of nearly 20 nm (Fig. 2(c)). These results suggested that the insertion of exogenous epitopes into the loop did not affect the self-assembly of the P domain into nanoparticles.

3.3 Humoral immune responses induced by nanoparticles in mice

Mice were immunized with the above nanoparticles three times at two-week intervals (Fig. 3(a)). The mice in the negative control groups were injected with PBS and PP. The levels of H16, M2e, and NP9 epitope-specific antibodies in serum were determined by ELISA two weeks after the third immunization (Figs. 3(b)–3(d)). As expected, the nanoparticles H16-PP, M2e-PP, and NP9-PP with three copies of a single epitope induced higher levels of epitope-specific antibodies than HMN-PP ($p < 0.05$), and the antibody titers were $(1.163 \pm 0.22) \times 10^5$, $(1.889 \pm 0.071) \times 10^5$, and $(6.18 \pm 0.48) \times 10^4$, respectively. This might be related to the number of epitopes present on the surface of nanoparticles.

Fc-mediated ADCC plays an important role in influenza protection and control of infection by clearing virus-infected cells. Raji cells infected with A/Hong Kong/2671(H3N2) were used as target cells, and the ADCC activity of serum was measured by flow cytometry (Fig. 3(e)). Except for the M2e-PP ($p < 0.001$) and HMN-PP ($p < 0.01$) groups, there was no significant difference in the ADCC response, indicating that the sera from mice immunized with the M2e epitope can induce ADCC in influenza virus-infected cells.

To evaluate the neutralizing activities of antibodies, neutralizing antibody titers against five influenza viruses in serum were measured using a CPE-based microneutralization assay (Fig. 3(f)). As expected, neither M2e-PP- nor NP9-PP-immunized mice had detectable neutralizing antibodies compared to the negative control group. The mice immunized with H16-PP not only had high titers of neutralizing antibodies against A/17/Perth/16/2009(H3N2) ($ID_{50} > 690$) and A/Hong Kong/2671/2019(H3N2) ($ID_{50} > 370$) but also had low titers of neutralizing antibodies against B/60/Massachusetts/20/2012 ($ID_{50} > 70$), illustrating that the H16 epitope was a potential dominant epitope that can induce broad-spectrum neutralizing antibodies. The mice immunized with HMN-PP showed slightly lower neutralizing antibody titers than those immunized with H16-PP. The data in this section indicated that NoV P particles as an antigen delivery system could induce a robust immune response against the target antigen.

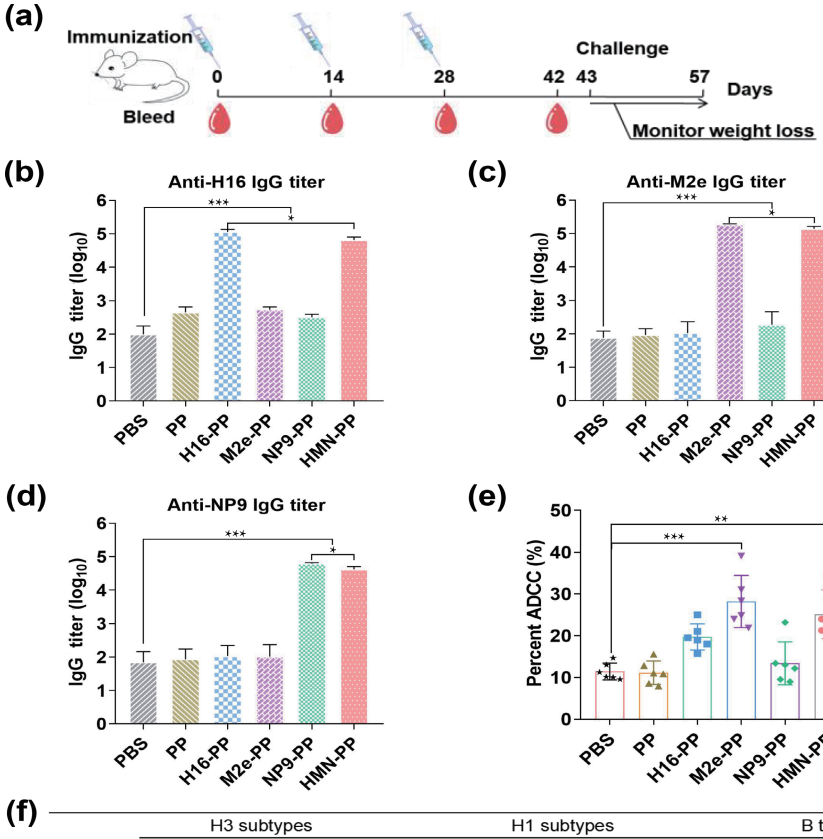

(f)

Serum samples	H3 subtypes		H1 subtypes		B type
	A/17/Perth/16/2009	A/HongKong/2671/2019	A/Guangdong-Maonan/SWL1536/2019	A/17/California/2009/38	B/60/Massachusetts/20/2012
PBS	< 20	< 20	< 20	< 20	< 20
PP	< 20	< 20	< 20	< 20	< 20
H16-PP	693.3	373.3	26.7	< 20	76.7
M2e-PP	< 20	< 20	< 20	< 20	< 20
NP9-PP	< 20	< 20	< 20	< 20	< 20
HMN-PP	346.7	240	20	< 20	43.3

Low titer — High titer
40 80 160 320 640

Figure 3 Humoral immune responses induced by multiepitope nanovaccines in mice. (a) Immunization and bleeding schedule of mice. (b)–(d) H16-, M2e-, and NP9-specific IgG titers in serum samples collected at week 6, $n = 6$. (e) ADCC responses in serum samples, $n = 6$. (f) ID_{50} values of mixed serum samples against influenza A and B viruses, $n = 6$.

3.4 Inclination of the Th1- or Th2-immune response induced by nanoparticles in mice

To explore the main type of immune response, we evaluated the IgG1/IgG2a ratios of serum samples by antibody typing assay (Fig. 4(a)). The IgG1/IgG2a ratios in the H16-PP and M2e-PP groups were > 1, corresponding to a trend to develop more Th2-biased immune responses. In contrast, the IgG1/IgG2a ratio in the NP9-PP group was < 1, suggesting that the NP9-PP immune group induced a Th1-biased immune response. Comparatively, the HMN-PP group induced a relatively balanced Th1/Th2 immune response.

To further verify the inclination of the immune response toward Th1- or Th2- biased immunity, we detected the amount of IFN-γ- or IL-4-secreting cells in splenocytes of immunized mice by ELISpot assays with IL-4 and IFN-γ as markers of Th2 and Th1 cells, respectively (Figs. 4(b) and 4(c)). After stimulation with the relevant peptide, splenocytes in the H16-PP and M2e PP groups tended to differentiate into IL-4-secreting cells ($p < 0.001$), while splenocytes in the NP9-PP group tended to differentiate into IFN-γ-secreting cells ($p < 0.001$). No significant differentiation was observed in the PBS and PP groups after stimulation with any peptide. The splenocytes in the HMN-PP group had no obvious tendency; that is, they could differentiate into IL-4-secreting cells when stimulated with H16 or M2e and into IFN-γ-secreting cells when stimulated with NP9, demonstrating a balanced Th1/Th2 immune response consistent with the IgG1/IgG2a ratio. The data in this section demonstrated that the inclination of the Th1- or Th2-immune response induced by the presented epitope might not be affected by NoV P particles as an antigen delivery system.

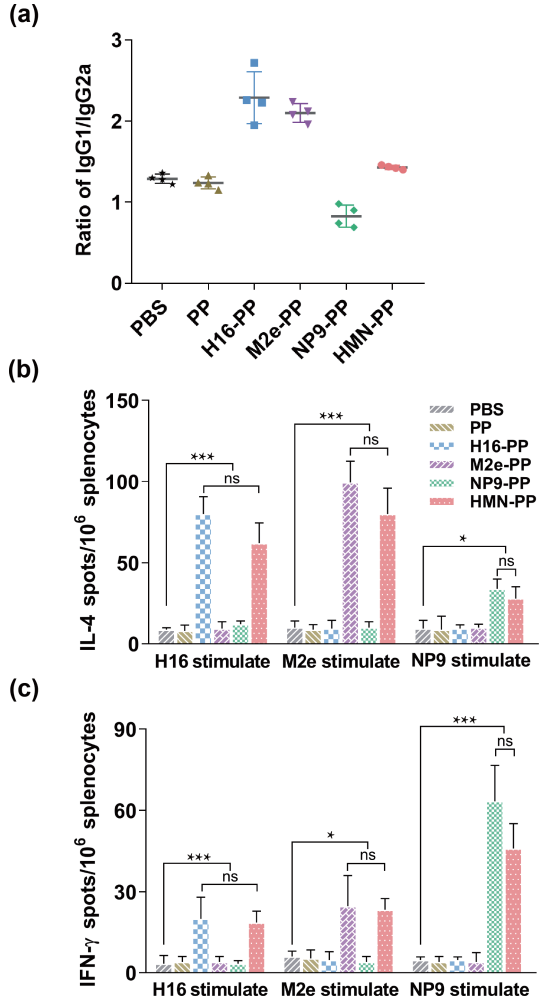

Figure 4 Analysis of the Th1/Th2 reaction in the immune response induced by multiepitope nanovaccines in mice. (a) IgG1/IgG2a ratios of serum samples, $n = 4$. (b) The IL-4- and (c) IFN-γ-secreting lymphocytes isolated from spleens were determined by ELISpot, $n = 6$.

3.5 Cellular immune responses induced by nanoparticles in mice

Lymphocyte proliferation is an important parameter for measuring the cellular immune response. Two weeks after the third immunization, splenic lymphocytes were stimulated with relevant peptides, and lymphocyte proliferation was measured by MTT assay. The proliferation level of epitope-specific lymphocytes was evaluated by the SI value (Fig. 5(a)). The H16-, M2e-, and NP9-stimulated SI of mice immunized with HMN-PP was higher than that of mice in the negative control groups but slightly lower than that of mice in the other experimental groups.

To further detect the activation level of T lymphocytes, the $CD3^+$ $CD4^+$ and $CD3^+$ $CD8^+$ T cells in the splenocyte population were analysed by flow cytometry (Figs. 5(b)–5(d)). The gating strategy for the splenocyte population was shown in Fig. S1 in the Electronic Supplementary Material (ESM). Compared with the negative control groups, significant activation of $CD3^+$ $CD4^+$ T cells was observed in the H16-PP, M2e-PP, NP9-PP, and HMN-PP groups ($p < 0.001$), especially in the HMN-PP group. Simultaneously, only the NP9-PP and HMN-PP groups ($p < 0.001$) induced a robust $CD3^+$ $CD8^+$ T-cell response. The activation of $CD3^+$ $CD8^+$ T cells was consistent with the inclination of the Th1- or Th2-immune response.

Peptide-specific CTL responses were evaluated by flow cytometry using an *in vivo* CTL assay. Compared with the negative control group, no detectable CTL response was observed in the H16-PP and M2e-PP groups (Fig. 5(e)). Mice immunized with NP9-PP exhibited the highest cytolytic activity ($p < 0.001$), followed by mice immunized with HMN-PP ($p < 0.01$). The CTL response results were consistent with the previous activation of $CD3^+$ $CD8^+$ T cells and proliferation of IFN-γ-secreting cells, indicating that the NP9 epitope was a T-cell epitope potentially capable of inducing CTL.

3.6 Evaluation of the protection from IAV challenge

To determine whether nanovaccines based on NoV P particles could protect mice from a lethal challenge, six mice in each group were challenged intranasally with H3N2 two weeks after the last immunization, and body weight and survival were monitored daily for 14 days (Figs. 6(a) and 6(b)). All mice in the negative control groups showed rapid weight loss and died within six days after the challenge, whereas the mice immunized with M2e-PP, H16-PP, and HMN-PP lost weight slowly, suggesting a prompt immune response. All mice immunized with M2e-PP survived ($p < 0.01$) with minimal weight loss (~ 10%), followed by the HMN-PP-immunized group ($p < 0.01$). The mice immunized with H16-PP and NP9-PP had significant weight loss (~ 20%), with 40% ($p < 0.05$) and 20% survival ($p > 0.05$) until day 14 after the challenge. To further determine whether nanovaccines induced a rapid adaptive immune response, the lungs were harvested for histopathological evaluation on day 4 post-challenge. Representative H&E staining of lung sections in each group is shown in Fig. 6(c) and Fig. S2 in the ESM. Histopathological evaluation was normal in the M2e-PP and HMN-PP groups. The lung tissue in the H16-PP group was mildly abnormal, showing only slightly thickened alveolar walls with some inflammatory cells, and that in the NP9-PP group was moderately abnormal with alveolar structure disorder and alveolar wall thickening. While the lung tissues in the negative control groups (PP and PBS groups) were severely abnormal, including alveolar structure

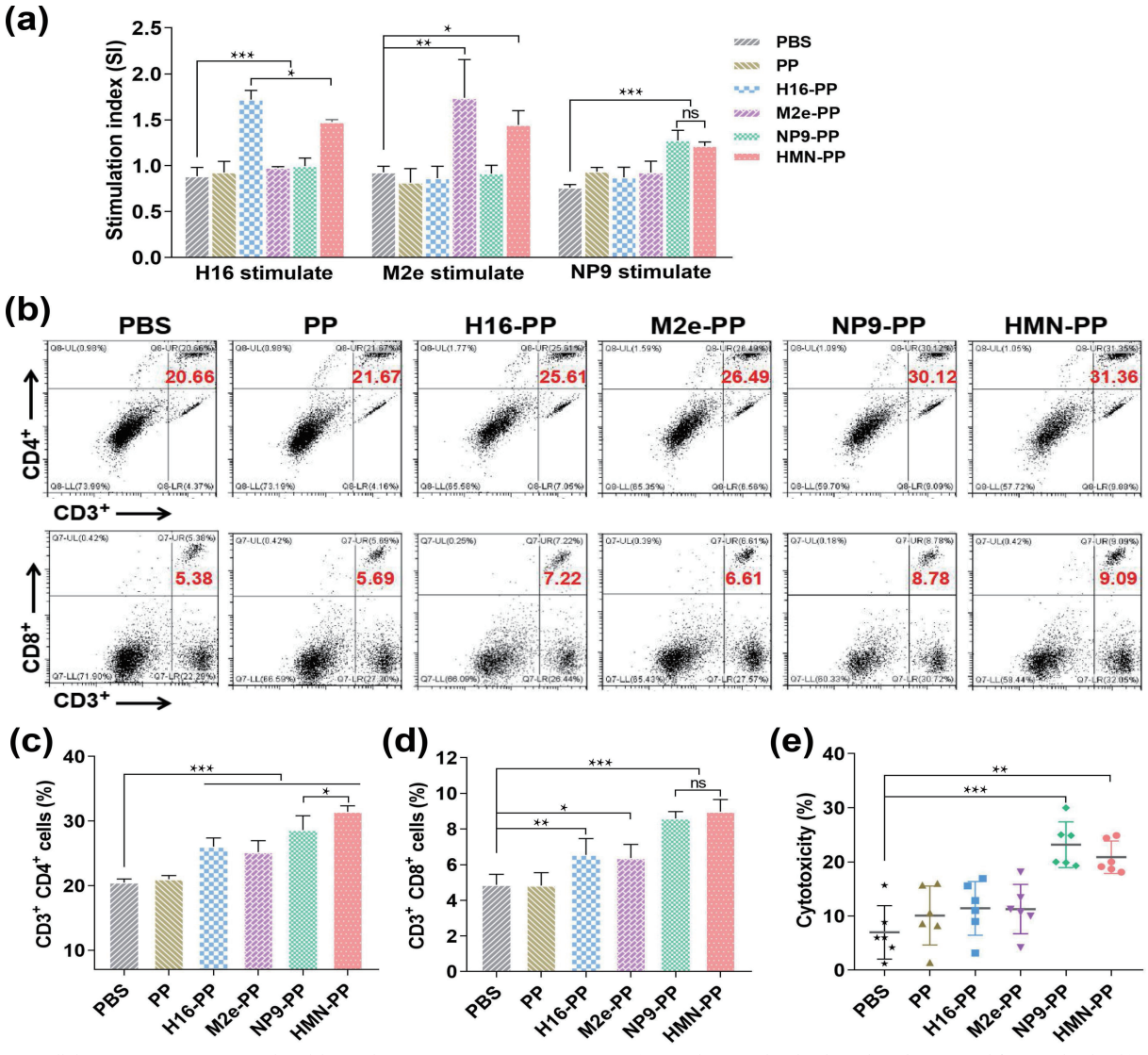

Figure 5 Cellular immune responses induced by multiepitope nanovaccines in mice. (a) Peptides-stimulated splenic lymphocyte proliferation levels. (b) Splenic lymphocytes isolated from mice immunized with nanovaccines were stained with anti-$CD3^+$, -$CD4^+$, and -$CD8^+$ mAbs, and analysed by flow cytometry. (c) Percentage of $CD3^+CD4^+$ T cells within splenic lymphocyte population, $n = 6$. (d) Percentage of $CD3^+CD8^+$ T cells within splenic lymphocyte population, $n = 6$. (e) Peptides-specific CTL responses of immunized mice, $n = 6$.

disorder, alveolar wall thickening, and a large number of necrotic cells and inflammatory cells in the alveolar cavity. M2e-PP and HMN-PP induced a rapid adaptive immune response to protect mice from H3N2.

3.7 Evaluation of long-term protection by antibodies

In view of the above results, the humoral immunity induced by H16 and M2e was essential in protecting the host against infections. Therefore, we further evaluated the ability of the nanovaccine to induce a long-lasting humoral immune response. Sera from immunized mice were collected at the 10th and 16th week after the primary immunization, and the epitope-specific antibody titers were determined by ELISA. There was no significant difference in epitope-specific antibody titers between the 10th and 16th week and the second week after the last immunization (Figs. 7(a)–7(c)), demonstrating the long-term stability of epitope-specific antibodies. Nanovaccines based on NoV P particles have irreplaceable advantages in inducing strong and long-lasting immune responses.

4 Discussion

Seasonal and pandemic influenza remains a serious threat to global health security, owing to its antigenic drift and antigenic shift [42]. There is an urgent need for effective vaccine strategies against highly variable influenza viruses. Although epitope vaccines have great potential to focus immune responses on conserved epitopes to broaden the breadth of protection, their low immunogenicity greatly limits their application in UIVs [43, 44]. Many studies have demonstrated that epitope vaccines may benefit from nanodelivery systems that mimic the size of pathogens and stably display multiple epitopes simultaneously [43, 45–47]. Self-assembled NoV P particles can be stably expressed on a large scale in *E. coli* and the surface loops can be modified to display foreign antigens efficiently, providing an ideal delivery platform for epitope vaccines.

In this study, we characterized and evaluated multiepitope nanovaccine candidates using conserved linear epitopes of HA, M2e, and NP conjugated with NoV P particles individually or in combination. As expected, the adjuvanted HMN-PP nanovaccine induced HA-specific neutralizing antibodies, an M2e-specific ADCC response, an NP-specific CTL response, and a relatively balanced Th1/Th2 immune response. We found that multiple epitopes conjugated with NoV P particles did not interfere with each other and that the inclination of the Th1- or Th2-immune response induced by the epitope might not be directly affected by

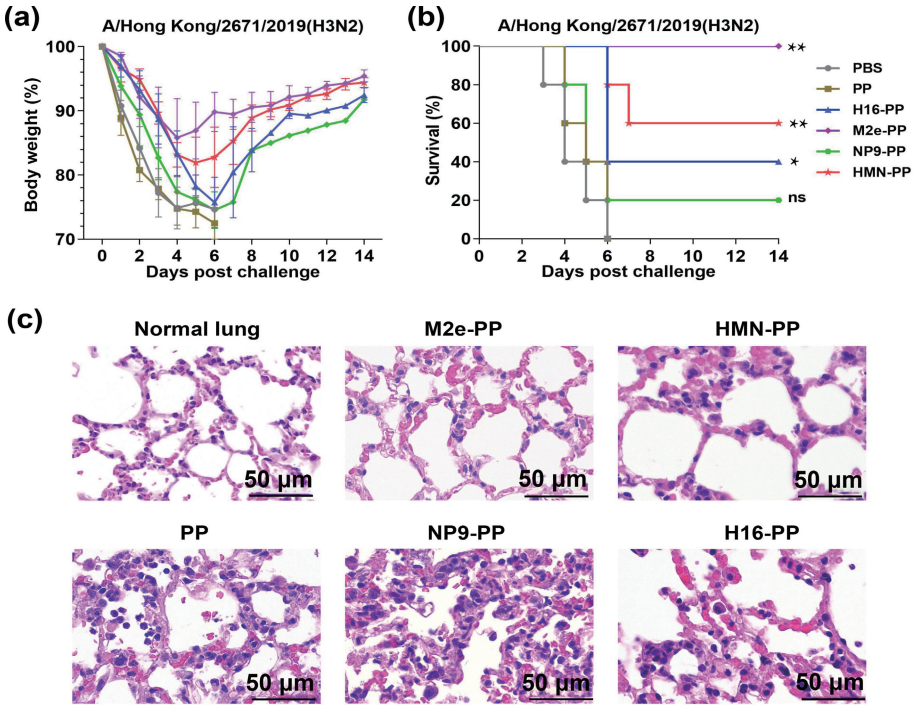

Figure 6 Protective efficacy against A/Hong Kong/2671/2019 (H3N2) challenge. (a) Body weight changes and (b) survival curves of influenza-infected mice, $n = 5$. (c) Representative H&E staining and histological analysis of lung tissue at 4 days post-infection. The normal lung section was used as a negative control.

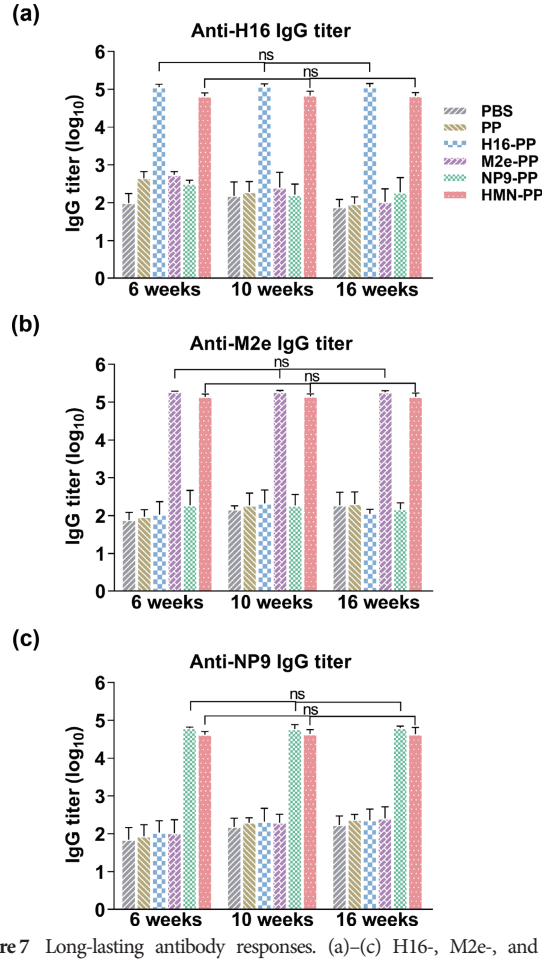

Figure 7 Long-lasting antibody responses. (a)–(c) H16-, M2e-, and NP9-specific antibody responses in serum samples at 6, 10, and 16 weeks after the first immunization, $n = 6$.

NoV P particles. Multiple copies of an epitope conjugated with an effective vaccine carrier stimulated stronger immune responses, as previously reported [48–50]. The generation of anti-epitope antibody might be antigen dose-dependent within a certain range. The HMN-PP nanovaccine induced a higher titer of H16-specific antibodies than H16-KLH or H16-MAP4 using the Freund adjuvant [19], illustrating that epitopes can be combined with nanotechnology to enhance immunogenicity. Notably, M2e-PP induced high levels of nonneutralizing antibodies to engage in ADCC responses and protected mice from lethal H3N2 challenge, which was comparable to the results of the ferritin [51, 52], CotB [53], and BP26 [54] nanoplatforms. In addition to neutralizing antibodies, nonneutralizing antibodies that can mediate ADCC also play an important role in protection from infection upon viral challenge [55, 56].

Cellular immunity is also beneficial in reducing the incidence of influenza infection, as reported [57]. Immune Targeting Systems Ltd. (UK) designed FP-01.1 nanoparticles (ClinicalTrials.gov identifier: NCT01265914), six conserved T-cell epitopes conjugated to fluorocarbon, to induce cellular responses to internal influenza A proteins [58]. Flu-v (ClinicalTrials.gov identifier: NCT01226758), including multiple highly conserved T-cell epitopes, elicits cellular immunity and reduces viral load [59, 60]. Here, HMN-PP and NP9-PP nanovaccines efficiently induced robust cellular immune responses, resulting in the proliferation of $CD4^+$ and $CD8^+$ T cells and NP9-specific CTL responses. Although NP9-PP induces strong cellular immunity, it is not sufficient to provide adequate protection when used alone. This attempt provides a reference for influenza vaccine candidates that induce cellular immunity.

Multimeric-001 (M-001) in a phase III clinical trial (ClinicalTrials.gov identifier: NCT03450915), a recombinant protein containing nine conserved epitopes from influenza A and B viruses, induces potent humoral and cellular immunity and provides broad strain coverage [61, 62]. The multiepitope nanovaccine HMN-PP in this study, consisting of three conserved epitopes of HA, M2e, and NP conjugated to the NoV P particle, similarly elicited both long-lasting humoral immunity and strong cellular immunity. The combination of epitope vaccines and the NoV P particle nanoplatforms is expected to further enhance immunogenicity and efficacy, which provides a promising idea for the design and optimization of vaccines.

5 Conclusions

In conclusion, this study demonstrated the feasibility of NoV P particles as a nanovaccine delivery vector to induce a potent and long-lasting immune response. We successfully constructed the multiepitope nanovaccines by fusing the conserved linear epitopes of HA, M2e, and NP to NoV P particles. The nanovaccines were prokaryotically expressed in mass in soluble form and self-assembled into nanoparticles. The mice immunized with HMN-PP exhibited strong cellular and humoral immune responses, and their specific antibody levels remained high after three months. In addition to neutralizing antibodies induced by the HA2 epitope, ADCC responses induced by M2e also protected mice from lethal influenza virus challenge. The multiepitope nanovaccine technology proposed in this study is promising for extending to the development of novel vaccines against highly variable viruses.

Acknowledgements

The current work was supported by the Department of Science and Technology of Jilin Province (Nos. 20220204008YY and 20210204197YY), and Changchun Science and Technology Bureau (No. 21ZY15).

References

[1] Bai, L.; Zhao, Y. L.; Dong, J. Z.; Liang, S. M.; Guo, M.; Liu, X. J.; Wang, X.; Huang, Z. X.; Sun, X. Y.; Zhang, Z. et al. Coinfection with influenza A virus enhances SARS-CoV-2 infectivity. *Cell Res.* **2021**, *31*, 395–403.

[2] Cao, K. L.; Wang, X.; Peng, H. R.; Ding, L. F.; Wang, X. W.; Hu, Y. Y.; Dong, L. L.; Yang, T. H.; Hong, X. J.; Xing, M. et al. A single vaccine protects against SARS-CoV-2 and influenza virus in mice. *J. Virol.* **2022**, *96*, e0157821.

[3] Parag, K. V.; du Plessis, L.; Pybus, O. G. Jointly inferring the dynamics of population size and sampling intensity from molecular sequences. *Mol. Biol. Evol.* **2020**, *37*, 2414–2429.

[4] Rahil, Z.; Leylek, R.; Schürch, C. M.; Chen, H.; Bjornson-Hooper, Z.; Christensen, S. R.; Gherardini, P. F.; Bhate, S. S.; Spitzer, M. H.; Fragiadakis, G. K. et al. Landscape of coordinated immune responses to H1N1 challenge in humans. *J. Clin. Invest.* **2020**, *130*, 5800–5816.

[5] Chen, J. R.; Liu, Y. M.; Tseng, Y. C.; Ma, C. Better influenza vaccines: An industry perspective. *J. Biomed. Sci.* **2020**, *27*, 33.

[6] Galli, C.; Orsi, A.; Pariani, E.; Lai, P. L.; Guarona, G.; Pellegrinelli, L.; Ebranati, E.; Icardi, G.; Panatto, D. In-depth phylogenetic analysis of the hemagglutinin gene of influenza A(H3N2) viruses circulating during the 2016–2017 season revealed egg-adaptive mutations of vaccine strains. *Expert Rev. Vaccines* **2020**, *19*, 115–122.

[7] Subbarao, K.; Barr, I. A tale of two mutations: Beginning to understand the problems with egg-based influenza vaccines? *Cell Host Microbe* **2019**, *25*, 773–775.

[8] Ping, J. H.; Lopes, T. J. S.; Nidom, C. A.; Ghedin, E.; Macken, C. A.; Fitch, A.; Imai, M.; Maher, E. A.; Neumann, G.; Kawaoka, Y. Development of high-yield influenza A virus vaccine viruses. *Nat. Commun.* **2015**, *6*, 8148.

[9] Dinis, J. M.; Florek, K. R.; Fatola, O. O.; Moncla, L. H.; Mutschler, J. P.; Charlier, O. K.; Meece, J. K.; Belongia, E. A.; Friedrich, T. C. Deep sequencing reveals potential antigenic variants at low frequencies in influenza a virus-infected humans. *J. Virol.* **2016**, *90*, 3355–3365.

[10] Morimoto, N.; Takeishi, K. Change in the efficacy of influenza vaccination after repeated inoculation under antigenic mismatch: A systematic review and meta-analysis. *Vaccine* **2018**, *36*, 949–957.

[11] Zeigler, D. F.; Gage, E.; Clegg, C. H. Epitope-targeting platform for broadly protective influenza vaccines. *PLoS One* **2021**, *16*, e0252170.

[12] Gschoesser, C.; Almanzar, G.; Hainz, U.; Ortin, J.; Schonitzer, D.; Schild, H.; Saurwein-Teissl, M.; Grubeck-Loebenstein, B. $CD4^+$ and $CD8^+$ mediated cellular immune response to recombinant influenza nucleoprotein. *Vaccine* **2002**, *20*, 3731–3738.

[13] Kumar, A.; Meldgaard, T. S.; Bertholet, S. Novel platforms for the development of a universal influenza vaccine. *Front. Immunol.* **2018**, *9*, 600.

[14] Kang, S. M.; Kim, M. C.; Compans, R. W. Virus-like particles as universal influenza vaccines. *Expert Rev. Vaccines* **2012**, *11*, 995–1007.

[15] Schwartzman, L. M.; Cathcart, A. L.; Pujanauski, L. M.; Qi, L.; Kash, J. C.; Taubenberger, J. K. An intranasal virus-like particle vaccine broadly protects mice from multiple subtypes of influenza a virus. *mBio* **2015**, *6*, e01044.

[16] Hu, C. M. J.; Chien, C. Y.; Liu, M. T.; Fang, Z. S.; Chang, S. Y.; Juang, R. H.; Chang, S. C.; Chen, H. W. Multi-antigen avian influenza a (H7N9) virus-like particles: Particulate characterizations and immunogenicity evaluation in murine and avian models. *BMC Biotechnol.* **2017**, *17*, 2.

[17] Park, Y. C.; Song, J. M. Preparation and immunogenicity of influenza virus-like particles using nitrocellulose membrane filtration. *Clin. Exp. Vaccine Res.* **2017**, *6*, 61–66.

[18] Gottlieb, T.; Ben-Yedidia, T. Epitope-based approaches to a universal influenza vaccine. *J. Autoimmun.* **2014**, *54*, 15–20.

[19] Gong, X.; Yin, H.; Shi, Y. H.; Guan, S. S.; He, X. Q.; Yang, L.; Yu, Y. J.; Kuai, Z. Y.; Jiang, C. L.; Kong, W. et al. Conserved stem fragment from H3 influenza hemagglutinin elicits cross-clade neutralizing antibodies through stalk-targeted blocking of conformational change during membrane fusion. *Immunol. Lett.* **2016**, *172*, 11–20.

[20] Gong, X.; Yin, H.; Shi, Y. H.; He, X. Q.; Yu, Y. J.; Guan, S. S.; Kuai, Z. Y.; Haji, N. M.; Haji, N. M.; Kong, W. et al. Evaluation of the immunogenicity and protective effects of a trivalent chimeric norovirus P particle immunogen displaying influenza HA2 from subtypes H1, H3 and B. *Emerg. Microbes Infect.* **2016**, *5*, 1–12.

[21] Smith, L. R.; Wloch, M. K.; Ye, M.; Reyes, L. R.; Boutsaboualoy, S.; Dunne, C. E.; Chaplin, J. A.; Rusalov, D.; Rolland, A. P.; Fisher, C. L. et al. Phase 1 clinical trials of the safety and immunogenicity of adjuvanted plasmid DNA vaccines encoding influenza A virus H5 hemagglutinin. *Vaccine* **2010**, *28*, 2565–2572.

[22] Qiao, Y. B.; Jin, S. H.; Nie, J. J.; Chang, Y. T.; Wang, B.; Guan, S. S.; Li, Q. H.; Shi, Y. H.; Kong, W.; Shan, Y. M. Hemagglutinin-based DNA vaccines containing trimeric self-assembling nanoparticles confer protection against influenza. *J. Leukoc. Biol.* **2022**, *112*, 547–556.

[23] Bahl, K.; Senn, J. J.; Yuzhakov, O.; Bulychev, A.; Brito, L. A.; Hassett, K. J.; Laska, M. E.; Smith, M.; Almarsson, Ö.; Thompson, J. et al. Preclinical and clinical demonstration of immunogenicity by mRNA vaccines against H10N8 and H7N9 influenza viruses. *Mol. Ther.* **2017**, *25*, 1316–1327.

[24] Hoelscher, M. A.; Garg, S.; Bangari, D. S.; Belser, J. A.; Lu, X. H.; Stephenson, I.; Bright, R. A.; Katz, J. M.; Mittal, S. K.; Sambhara, S. Development of adenoviral-vector-based pandemic influenza vaccine against antigenically distinct human H5N1 strains in mice. *Lancet* **2006**, *367*, 475–481.

[25] Kim, E. H.; Han, G. Y.; Nguyen, H. An adenovirus-vectored influenza vaccine induces durable cross-protective hemagglutinin stalk antibody responses in mice. *Viruses* **2017**, *9*, 234.

[26] Kamlangdee, A.; Kingstad-Bakke, B.; Anderson, T. K.; Goldberg, T. L.; Osorio, J. E. Broad protection against avian influenza virus by using a modified vaccinia Ankara virus expressing a mosaic hemagglutinin gene. *J. Virol.* **2014**, *88*, 13300–13309.

[27] Gurwith, M.; Lock, M.; Taylor, E. M.; Ishioka, G.; Alexander, J.; Mayall, T.; Ervin, J. E.; Greenberg, R. N.; Strout, C.; Treanor, J. J. et al. Safety and immunogenicity of an oral, replicating adenovirus serotype 4 vector vaccine for H5N1 influenza: A randomised, double-blind, placebo-controlled, phase 1 study. *Lancet Infect. Dis.* **2013**, *13*, 238–250.

[28] Dhakal, S.; Loube, J.; Misplon, J. A.; Lo, C. Y.; Creisher, P. S.; Mulka, K. R.; Deshpande, S.; Mitzner, W.; Klein, S. L.; Epstein, S. L. Effect of an adenovirus-vectored universal influenza virus vaccine on pulmonary pathophysiology in a mouse model. *J. Virol.* **2021**, *95*, e02359–20.

[29] Toussaint, N. C.; Kohlbacher, O. OptiTope—A web server for the

selection of an optimal set of peptides for epitope-based vaccines. *Nucleic Acids Res.* **2009**, *37*, W617–W622.
[30] Skwarczynski, M.; Toth, I. Peptide-based synthetic vaccines. *Chem. Sci.* **2016**, *7*, 842–854.
[31] Thompson, C. P.; Lourenço, J.; Walters, A. A.; Obolski, U.; Edmans, M.; Palmer, D. S.; Kooblall, K.; Carnell, G. W.; O'Connor, D.; Bowden, T. A. et al. A naturally protective epitope of limited variability as an influenza vaccine target. *Nat. Commun.* **2018**, *9*, 3859.
[32] Walls, A. C.; Fiala, B.; Schäfer, A.; Wrenn, S.; Pham, M. N.; Murphy, M.; Tse, L. V.; Shehata, L.; O'Connor, M. A.; Chen, C. B. et al. Elicitation of potent neutralizing antibody responses by designed protein nanoparticle vaccines for SARS-CoV-2. *Cell* **2020**, *183*, 1367–1382.e17.
[33] Ko, C. N.; Zang, S. H.; Zhou, Y. T.; Zhong, Z. F.; Yang, C. Nanocarriers for effective delivery: Modulation of innate immunity for the management of infections and the associated complications. *J. Nanobiotechnol.* **2022**, *20*, 380.
[34] Huang, X.; Kon, E.; Han, X.; Zhang, X.; Kong, N.; Mitchell, M. J.; Peer, D.; Tao, W. Nanotechnology-based strategies against SARS-CoV-2 variants. *Nat. Nanotechnol.* **2022**, *17*, 1027–1037.
[35] Deng, L.; Wang, B. Z. A perspective on nanoparticle universal influenza vaccines. *ACS Infect. Dis.* **2018**, *4*, 1656–1665.
[36] Sun, Y.; Guo, Y. Q.; Feng, X. J.; Fu, L.; Zheng, Y. Y.; Dong, Y.; Zhang, Y.; Yu, X. H.; Kong, W.; Wu, H. Norovirus P particle-based tau vaccine-generated phosphorylated tau antibodies markedly ameliorate tau pathology and improve behavioral deficits in mouse model of Alzheimer's disease. *Sig. Transduct. Target. Ther.* **2021**, *6*, 61.
[37] Ghorbani, A.; Ngunjiri, J. M.; Xia, M.; Elaish, M.; Jang, H.; Mahesh, K. C.; Abundo, M. C.; Jiang, X.; Lee, C. W. Heterosubtypic protection against avian influenza virus by live attenuated and chimeric norovirus P-particle-M2e vaccines in chickens. *Vaccine* **2019**, *37*, 1356–1364.
[38] Jiang, L. P.; Fan, R. J.; Sun, S. Y.; Fan, P. H.; Su, W. H.; Zhou, Y.; Gao, F.; Xu, F.; Kong, W.; Jiang, C. L. A new EV71 VP3 epitope in norovirus P particle vector displays neutralizing activity and protection *in vivo* in mice. *Vaccine* **2015**, *33*, 6596–6603.
[39] Tan, M.; Jiang, X. Norovirus P particle: A subviral nanoparticle for vaccine development against norovirus, rotavirus and influenza virus. *Nanomedicine (Lond)* **2012**, *7*, 889–897.
[40] Yu, Y. J.; Fu, L.; Shi, Y. H.; Guan, S. S.; Yang, L.; Gong, X.; Yin, H.; He, X. Q.; Liu, D. N.; Kuai, Z. Y. et al. Elicitation of HIV-1 neutralizing antibodies by presentation of 4E10 and 10E8 epitopes on norovirus P particles. *Immunol. Lett.* **2015**, *168*, 271–278.
[41] Tan, M.; Huang, P. W.; Xia, M.; Fang, P. A.; Zhong, W. M.; McNeal, M.; Wei, C.; Jiang, W.; Jiang, X. Norovirus P particle, a novel platform for vaccine development and antibody production. *J. Virol.* **2011**, *85*, 753–764.
[42] Horby, P. Improving preparedness for the next flu pandemic. *Nat. Microbiol.* **2018**, *3*, 848–850.
[43] De Brito, R. C. F.; De O. Cardoso, J. M.; Reis, L. E. S.; Vieira, J. F.; Mathias, F. A. S.; Roatt, B. M.; Aguiar-Soares, R. D. D. O.; Ruiz, J. C.; De M. Resende, D.; Reis, A. B. Peptide vaccines for leishmaniasis. *Front. Immunol.* **2018**, *9*, 1043.
[44] Yang, H.; Kim, D. S. Peptide immunotherapy in vaccine development: From epitope to adjuvant. *Adv. Protein Chem. Struct. Biol.* **2015**, *99*, 1–14.
[45] Varypataki, E. M.; Silva, A. L.; Barnier-Quer, C.; Collin, N.; Ossendorp, F.; Jiskoot, W. Synthetic long peptide-based vaccine formulations for induction of cell mediated immunity: A comparative study of cationic liposomes and PLGA nanoparticles. *J. Control. Release* **2016**, *226*, 98–106.
[46] Kang, Y. F.; Sun, C.; Zhuang, Z.; Yuan, R. Y.; Zheng, Q. B.; Li, J. P.; Zhou, P. P.; Chen, X. C.; Liu, Z.; Zhang, X. et al. Rapid development of SARS-CoV-2 spike protein receptor-binding domain self-assembled nanoparticle vaccine candidates. *ACS Nano* **2021**, *15*, 2738–2752.
[47] Han, S. L.; Ma, W. Y.; Jiang, D. W.; Sutherlin, L.; Zhang, J.; Lu, Y.; Huo, N.; Chen, Z.; Engle, J. W.; Wang, Y. P. et al. Intracellular signaling pathway in dendritic cells and antigen transport pathway *in vivo* mediated by an OVA@DDAB/PLGA nano-vaccine. *J. Nanobiotechnol.* **2021**, *19*, 394.
[48] Jones, K. L.; Pride, M. C.; Edmiston, E.; Yang, M.; Silverman, J. L.; Crawley, J. N.; Van De Water, J. Autism-specific maternal autoantibodies produce behavioral abnormalities in an endogenous antigen-driven mouse model of autism. *Mol. Psychiatry* **2020**, *25*, 2994–3009.
[49] Schickli, J. H.; Whitacre, D. C.; Tang, R. S.; Kaur, J.; Lawlor, H.; Peters, C. J.; Jones, J. E.; Peterson, D. L.; McCarthy, M. P.; Van Nest, G. et al. Palivizumab epitope-displaying virus-like particles protect rodents from RSV challenge. *J. Clin. Invest.* **2015**, *125*, 1637–1647.
[50] Molino, N. M.; Neek, M.; Tucker, J. A.; Nelson, E. L.; Wang, S. W. Viral-mimicking protein nanoparticle vaccine for eliciting anti-tumor responses. *Biomaterials* **2016**, *86*, 83–91.
[51] Qi, M.; Zhang, X. E.; Sun, X. X.; Zhang, X. W.; Yao, Y. F.; Liu, S. L.; Chen, Z.; Li, W.; Zhang, Z. P.; Chen, J. J. et al. Intranasal nanovaccine confers homo- and hetero-subtypic influenza protection. *Small* **2018**, *14*, 1703207.
[52] Qiao, Y. B.; Zhang, Y. X.; Chen, J.; Jin, S. H.; Shan, Y. M. A biepitope, adjuvant-free, self-assembled influenza nanovaccine provides cross-protection against H3N2 and H1N1 viruses in mice. *Nano Res.* **2022**, *15*, 8304–8314.
[53] Zhao, G. Y.; Miao, Y.; Guo, Y.; Qiu, H. J.; Sun, S. H.; Kou, Z. H.; Yu, H.; Li, J. F.; Chen, Y.; Jiang, S. B. et al. Development of a heat-stable and orally delivered recombinant M2e-expressing *B. subtilis* spore-based influenza vaccine. *Hum. Vaccin. Immunother.* **2014**, *10*, 3649–3658.
[54] Kang, S.; Kim, Y.; Shin, Y.; Song, J. J.; Jon, S. Antigen-presenting, self-assembled protein nanobarrels as an adjuvant-free vaccine platform against influenza virus. *ACS Nano* **2021**, *15*, 10722–10732.
[55] Ackerman, M. E.; Das, J.; Pittala, S.; Broge, T.; Linde, C.; Suscovich, T. J.; Brown, E. P.; Bradley, T.; Natarajan, H.; Lin, S. et al. Route of immunization defines multiple mechanisms of vaccine-mediated protection against SIV. *Nat. Med.* **2018**, *24*, 1590–1598.
[56] Schepens, B.; Sedeyn, K.; Vande Ginste, L.; De Baets, S.; Schotsaert, M.; Roose, K.; Houspie, L.; Van Ranst, M.; Gilbert, B.; Van Rooijen, N. et al. Protection and mechanism of action of a novel human respiratory syncytial virus vaccine candidate based on the extracellular domain of small hydrophobic protein. *EMBO Mol. Med.* **2014**, *6*, 1436–1454.
[57] Bonduelle, O.; Carrat, F.; Luyt, C. E.; Leport, C.; Mosnier, A.; Benhabiles, N.; Krivine, A.; Rozenberg, F.; Yahia, N.; Samri, A. et al. Characterization of pandemic influenza immune memory signature after vaccination or infection. *J. Clin. Invest.* **2014**, *124*, 3129–3136.
[58] Francis, J. N.; Bunce, C. J.; Horlock, C.; Watson, J. M.; Warrington, S. J.; Georges, B.; Brown, C. B. A novel peptide-based pan-influenza A vaccine: A double blind, randomised clinical trial of immunogenicity and safety. *Vaccine* **2015**, *33*, 396–402.
[59] Pleguezuelos, O.; Robinson, S.; Fernandez, A.; Stoloff, G. A.; Caparrós-Wanderley, W. Meta-analysis and potential role of preexisting heterosubtypic cellular immunity based on variations in disease severity outcomes for influenza live viral challenges in humans. *Clin. Vaccine Immunol.* **2015**, *22*, 949–956.
[60] Pleguezuelos, O.; Robinson, S.; Fernández, A.; Stoloff, G. A.; Mann, A.; Gilbert, A.; Balaratnam, G.; Wilkinson, T.; Lambkin-Williams, R.; Oxford, J. et al. A synthetic influenza virus vaccine induces a cellular immune response that correlates with reduction in symptomatology and virus shedding in a randomized phase Ib live-virus challenge in humans. *Clin. Vaccine Immunol.* **2015**, *22*, 828–835.
[61] Phillipson, J. E.; Babecoff, R.; Ben-Yedidia, T. Is a universal influenza vaccine feasible? *Adv. Vaccines Immunother.* **2019**, *7*, 2515135519885547.
[62] Van Doorn, E.; Liu, H.; Ben-Yedidia, T.; Hassin, S.; Visontai, I.; Norley, S.; Frijlink, H. W.; Hak, E. Evaluating the immunogenicity and safety of a BiondVax-developed universal influenza vaccine (Multimeric-001) either as a standalone vaccine or as a primer to H5N1 influenza vaccine: Phase IIb study protocol. *Medicine (Baltimore)* **2017**, *96*, e6339.